How Reverse Reactions Influence the Yield of Self-Assembly Robots

Shuhei Miyashita, Maurice Göldi, and Rolf Pfeifer *

Abstract

The decay in structure size of manufacturing products has yielded new demands on spontaneous composition methods. The key for the realization of small-sized robots lies in how to achieve the efficient assembly sequence in a bottom-up manner, where most of the parts have only limited (or no) computational (i.e. deliberative) abilities. In this paper, based on a novel self-assembly platform consisting of self-propulsive cm-sized modules capable of aggregation on the surface of water, we study the effect of stochasticity and morphology with respect to the yield of targeted formations in self-assembly processes. Specifically, we focused on a unique phenomenon that a number of modules instantly compose a target product without forming intermediate subassemblies, some of which constitute undesired geometrical formations (termed one-shot aggregation). Together with a focus on the role that the morphology (shape) of the modules plays, we validate the effect of one-shot aggregation with kinetic rate mathematical model. Moreover, we examined the degree of parallelism of the assembly process, which is an essential factor in self-assembly, but is not systematically taken into account by existing frameworks.

keywords: self-propulsive self-assembly robot; stochasticity; reverse reaction; morphology; one-shot aggregation; yield problem; degree of parallelism; distributed system.

1 Introduction

Manufacturing technologies and industries heavily rely on robots. For macroscopic objects industrial robots are not only economical but are also reliable, fast, and accurate. Such robots, however, hit a barrier – entailing lower yields and higher fabrication costs – as the assembled objects become smaller/complex, and the assembly environments become increasingly inaccessible. One potential solution to this problem is to exploit processes of self-assembly, that is, processes in which the interaction of pre-existing components leads to organized structures without human intervention. Such components could be, for instance, identical mechanical units (modules).

*Shuhei Miyashita, Maurice Göldi, and Rolf Pfeifer are with the Artificial Intelligence Laboratory, University of Zurich, Switzerland. miya@ifi.uzh.ch

Self-assembly is known to be of crucial importance in the biological realm at all scales. For instance, the formation of the complex symmetrical protein shells of spherical viruses is a well-studied example of self-assembly. The shell of the T4 bacteriophage (so-called because it infects bacteria) is composed of hundreds of parts and it is not plausible to assume that the instructions for its construction are contained only in the genetic material of the virus. The organism consists of about 70 different kinds of proteins and exploits the metabolism of the host cell (e.g. E. Coli) to generate the copies of itself (Leiman et al. 2003; Zlotnick 2005). Moreover, it is truly remarkable that if the right kinds of proteins are mixed, the virus can be synthesized *in vitro*. Although the discussion of whether or not viruses are living things has been controversial ever since they were first discovered, they are generally considered to be non-living entities because they cannot reproduce without the help of a host organism. As the research outlined above shows, the rules that govern interactions at a local level are simple; the interactions of a large number of entities can lead to the emergence of complex structures through a process of self-assembly.

In order to develop a better formal understanding of the general principles underlying self-assembly, many attempts have been made to create descriptive models. Pioneering experiments on artificial self-replication were conducted by Lionel and Roger Penrose almost 50 years ago (Penrose 1959). They presented a mechanical model of natural self-replication in a stochastic environment. Hosokawa's work (Hosokawa et al. 1994, 1996) in the 1990's followed this stream, examining the clustering pattern of passive elements. The group of Whitesides revealed different types of self-assembly at small scales (Bowden et al. 1997; Grzybowski et al. 2000, 2003, 2004). Notable ideas about conformational switch (physics based internal state of a component) were proposed by Saitou (Saitou 1999).

Recent advances in robotics have highlighted the importance of self-assembly for building complex objects, aimed at exploiting the obvious advantages of living organisms. Modular robots – autonomous machines typically consisting of homogeneous building blocks – promise a viable solution because they have the ability to be highly versatile. For instance, at least ideally, they can re-configure and adapt their shape according to a given task-environment. Work has mainly been focused on the design and construction of the basic building blocks of a typically small repertoire, with docking interfaces, which allow transfer of mechanical forces, moments and electrical power, and which can also be used for data communication (Fukuda and Kawauch 1990; Nakano et al. 1994; Chirikjian 1994; Murata et al. 1994, 1998, 1999; Yim 1994; Kotay et al. 1998; Rus and Vona 2001; Mondada et al. 2005; Christensen et al. 2007; Castano et al. 2002; Jorgensen et al. 2004; Zykov et al. 2005).

To date, a few self-reconfigurable modular robots relying on stochastic self-assembly have been built (White et al. 2004, 2005; Shimizu et al. 2005; Klavins 2007; Bishop et al. 2005; Griffith et al. 2005). Novel applications in the medical field have recently been suggested. Edible "robotic tablets" that assemble in the stomach (Nagy et al. 2008; Harada et al. 2009), and drug blending *in vivo* by autonomous micro sized capsules (Leong et al. 2006) illustrate the potential of stochastic self-assembly robots. The main difference from existing modular robotics is the way in which the modules are supplied. The robot or formed cluster waits for a supplemental module to be "delivered" from the environment, rather than supplying it itself. In all these systems the units in-

teract asynchronously during their assembly processes and concurrently once they have aggregated. Nevertheless, a certain amount of state-based control is still required for the modules to move, communicate, and dock. Generally, the internal representations of the module's configurations, such as rewritable look-up tables, follow the same lines as conventional approaches.

By taking tools and methods from nature, many inroads have already been made in utilizing self-assembly for the fabrication of structures at molecular scales (Winfree et al. 1998; Seeman 2003; Mao et al. 2000; Shih et al. 2004; Rothemund 2006; Yokoyama et al. 2001). These methods are powerful and effective, especially due to the exploitation of the advantages of small scales, e.g. the ability to control stochasticity through temperature during mass production of the assembled units. An essentially analogous problem to the macroscopic approaches has been investigated in the context of DNA folding where one of the objectives is to increase the yield of self-assembly processes (Rothemund 2006). Similarly, a lot of research effort is being devoted to the development of high-yield procedures for integration and mass manufacturing of heterogeneous systems via self-assembly of mesoscopic and macroscopic components (Boncheva et al. 2003; Gracias et al. 2000; Wolfe et al. 2003). The disadvantage of such an approach may be, if anything, that the assembly parts that can be employed are limited to what naturally exist or are manufacturable at the scale in question. In molecular assembly, three conditions are known to be necessary: weak interaction, thermal agitation, and nucleation. The mechanism behind molecular assembly is numerous trial and error iterations of the connections until the strength reaches a sustainable level. This is one of the fundamental differences from pick-and-place style (deterministic) assembly. Through such a process, the system gradually shifts to a more energetically stable state. In artificial self-assembly systems at the macro-scale, compared to molecular assembly, the frequency of collisions has a practical limit due especially to the inertial effect.

In this paper, motivated by the outstanding potential need for realizing effective self-assembly system, we set the goal of this study to investigate the role of stochasticity and morphology on self-assembly and propose the novel approach that can be used in versatile scales. We made the following set of prerequisites for establishing the experimental conditions.

1. **The system should be "stochastic" and "distributed" with all components being autonomously assembled in parallel.** Small-scale self-assembly systems that appear in nature, such as molecular reactions, are considered to be distributed systems in stochastic environment, implying that there are uncertainties in the global information concerning the components, e.g. locations and total number of modules. Therefore, the model should be compatible with molecular systems to some degree.

2. **The components should have only limited (or no) computational (decisive) abilities but be self-sufficient.** Once a set of experimental conditions is invoked, modules are expected to act independently (be untethered), following local causal rules imposed by the environment, in terms of actuation (self-propulsion) and power.

3. **The module architecture should be scalable.** Based on the fact that self-assembly must take place on a small scale in order to achieve

environmental stochasticity, the module design should be scalable and simple.

In the following Section 2, we introduce the proposed experimental setup and describe its behavior. In Section 3, we estimate the convergence of the model based on kinetic rate calculations. We further examine the observed aggregation pattern employing the notion of *degree of parallelism* in Section 4. In Section 5 we present our conclusions.

2 The model: self-propulsive modules

2.1 Modules and experimental setup

The term "self-assembly" implies that the elements or parts involved assemble in a spontaneous manner without external intervention or control. Such behavior is typical of dissipative systems. Taking this into account, we chose to produce a set of modules with different shapes that swarm on water.

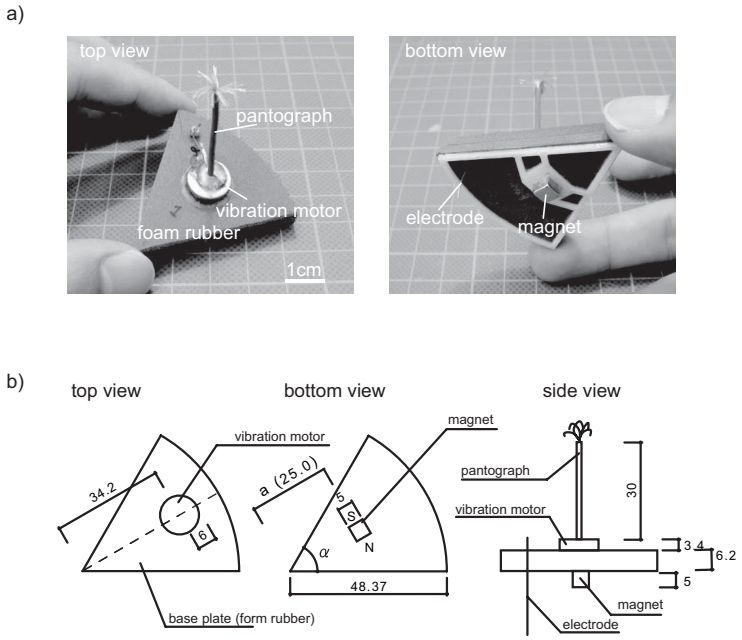

Figure 1: A self-propulsive module. (a) Photographs of an individual module. (b) Schematic representation of the module (units: $[mm]$). Each module weighs $2.8\,g$ and has a footprint of $12.25\,cm^2$.

The modules, which we call *Tribolon*[1], are equipped with a flat coreless vibration motor (T.P.C DC MOTOR FM34F, $12000 \sim 14000\,rpm\,(2.5 - 3.5\,Volts)$) on the top of the base plate to allow self-propulsion, and a single permanent magnet (flux density $1.3\,T$, $5\times5\times5\,mm^3$) at the bottom for attractive/repulsive interactions (Figure 2). This allowed the modules to jiggle and move around in their environment. The "shape" of the modules can be characterized by a set

[1] derived from Tribology

of angles and lengths. However, an inevitable problem which arises is that a change in one parameter can lead to changes in other parameters, which makes it difficult to discuss the implications of a single parameter change. Here, in order to minimize this problem, we chose a circular-sector-shaped tiles spanning an angle α ($\alpha = 60°$ in Figure 1). The characteristics of this shape is that it sustains geometric similarity irrespective to the change of the angle.

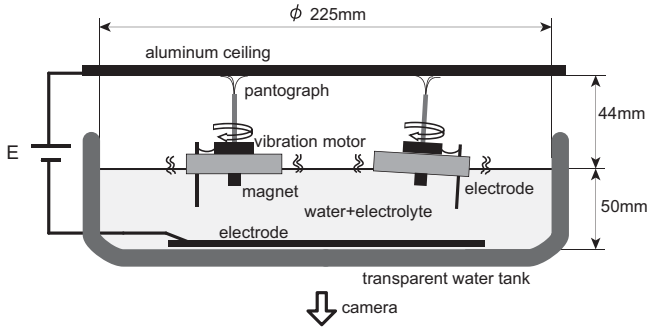

Figure 2: Illustration of the experimental environment with two modules.

As a power supply, rather than using batteries for each module, we opted to supply electricity through a pantograph that draws current from a metallic ceiling (Figure 2). When an electrical potential is applied to the ceiling plate, current flows through the pantograph to the vibration motor, returning to ground via electrodes immersed in the conductive water (salt solution). Due to this setup, all modules receive the same constant power and they can be lightweight ($2.8\,g$ each), which would not be the case if batteries were used.

The salt solution ($83.3\,g/l$) can generate current flow by the chemical reactions in Eq. (1).

$$2\mathrm{NaCl} + \mathrm{H_2O} \rightarrow \mathrm{H_2} \uparrow + \mathrm{Cl_2} \uparrow + 2\mathrm{NaOH} \tag{1}$$

The concentration of the salt solution is sufficient to sustain current flow during the entire course of the experiment. In order to avoid chemical deposition onto the electrodes, we used platinum for the electrode material. The base plate is made of foam rubber to produce a certain amount of friction. We set a camera below the tank and observed the modules through the transparent bottom.

2.2 Magnetism

Given N as the number of hard magnets existing in the system, the force ($\boldsymbol{F}_{ij}$) and the torque ($\boldsymbol{\tau}_{ij}$) experienced by i-th magnet by interacting with j-th magnet ($i, j \in$N) can be expressed and simplified as:

$$\boldsymbol{F}_{ij} = \mu_0 \int_{vi} (\boldsymbol{M}_i \cdot \nabla)\, \boldsymbol{H}_j \, dv \approx \mu_0 v_i (\boldsymbol{M}_i \cdot \nabla) \boldsymbol{H}_j \tag{2}$$

$$\boldsymbol{\tau}_{ij} = \mu_0 \int_{vi} (\boldsymbol{M}_i \times \boldsymbol{H}_j)\, dv \approx \mu_0 v_i \boldsymbol{M}_i \times \boldsymbol{H}_j \tag{3}$$

where $\boldsymbol{H}_j$ is the magnetic field exerted by j-th magnet, $\mu_0 = 4\pi \times 10^{-7}$ (Tm/A) is the permeability of free space, v_i and $\boldsymbol{M}_i$ are the volume and the magnetization of i-th magnet, respectively.

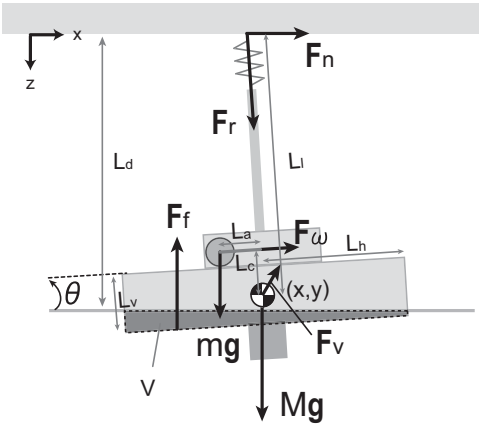

Figure 3: Schematic of a single module.

m	Mass of the eccentric weight
M	Mass of the module body
I	Moment of inertia around the center of mass
θ	Rotational angle of the module
$\boldsymbol{F}_\omega$	Centripetal force
$\boldsymbol{F}_n$	Frictional force
$\boldsymbol{F}_r$	Resistive force
$\boldsymbol{F}_f$	Buoyancy force
$\boldsymbol{F}_v$	Viscous force
$\boldsymbol{g}$	Gravitational acceleration vector
L_a	Amplitude of eccentric mass rotation
L_l	Natural length between center of mass and the ceiling
L_h	Radius of the module
L_v	Height of the module
L_c	Distance between center of mass and center of vibration motor
L_d	Distance between the ceiling and water

The magnetic field created by j-th magnet with respect to the position $\boldsymbol{r}$ can be described as

$$\boldsymbol{H}_j(\boldsymbol{r}) = \frac{1}{4\pi|\boldsymbol{r}^3|}\Big(\frac{3(\boldsymbol{m_j}\cdot\boldsymbol{r})\boldsymbol{r}}{|\boldsymbol{r}|^2} - \boldsymbol{m_j}\Big) \tag{4}$$

where $\boldsymbol{m_j} = v_j\boldsymbol{M}_j$.

Utilizing $\boldsymbol{H}$, the total magnetic potential energy of the system (U_{total}) can be described as

$$U_{total} \quad = \quad -\frac{\mu_0}{2}\sum_{i,j\ i\neq j}^{N}\int_v \boldsymbol{M}_i\cdot\boldsymbol{H}_j\,dv \tag{5}$$

We normalize the energy as $U'_{total} \equiv U_{total}/(\frac{\mu_0}{4\pi}v^2M^2)$ assuming all the magnets are equally magnetized.

2.3 Model of motion

The long range interaction described above is identical for each type of module, regardless of its shape, because identical magnets were used. However, the short range interaction, i.e. the final alignment, is dominated by shape and this was experimentally investigated. For the sake of simplicity, we consider the motion of a module in two dimensions (Figure 3). Note that the modules could tilt, inducing rather large fluctuations in the current flowing through the motors.

Let $\boldsymbol{x} = [x, z]^T$ be a position vector in a Cartesian coordinate system. Transitional and rotational motions can then be described by Eq. (6) and Eq. (7), respectively.

$$M\ddot{\boldsymbol{x}} \quad = \quad \boldsymbol{F}_\omega + \boldsymbol{F}_r + \boldsymbol{F}_f + \boldsymbol{F}_n + \boldsymbol{F}_v + (M+m)\boldsymbol{g} \tag{6}$$

$$I\ddot{\theta} \quad = \quad \boldsymbol{r}_\omega\times\boldsymbol{F}_\omega + \boldsymbol{r}_\omega\times m\boldsymbol{g} + \boldsymbol{r}_f\times\boldsymbol{F}_f + \boldsymbol{r}_n\times\boldsymbol{F}_n \tag{7}$$

where $\boldsymbol{r}_\omega$, $\boldsymbol{r}_f$, $\boldsymbol{r}_n$, and $\boldsymbol{r}_v$ are directional vectors from the center of mass of the module to the action points $\boldsymbol{F}_\omega$, $\boldsymbol{F}_f$, $\boldsymbol{F}_n$, and $\boldsymbol{F}_v$, respectively. Each force can

be simplified as:

$$
\begin{aligned}
F_\omega &= mL_a\omega^2\cos(\omega T+\phi) && (8)\\
F_r &\approx -k(\frac{y}{\cos\theta}-L_l) && (9)\\
F_n &= \mu F_r\cos\theta \approx -\mu k(y-L_l\cos\theta) && (10)\\
F_f &= -Vg && (11)\\
\boldsymbol{F}_v &\approx -c\dot{\boldsymbol{x}} && (12)
\end{aligned}
$$

where ϕ specifies the initial phase of the eccentric mass, V is the volume of foam rubber that is under water, k is the spring constant of the pantograph, μ is the kinetic frictional coefficient, T is time, and c is the coefficient of viscosity of the salt water. What is important here is that the rotational speed of the eccentric mass is quasi proportional to the voltage applied. As this speed increases, it leads to faster movement of the modules and stronger collisions between them. The treatment of the precise motion of a module shall be extended in future work.

Figure 4 shows snapshots of the characteristic trajectories of two modules during a 9-*sec* interval. Module 1 strikes module 2 while being attracted by the magnetic force between them. It should be noted that due to the rotation of the eccentric mass, each module repels other modules along a certain direction. Moreover, because the repulsion force varies, the modules change their relative positions frequently (illustrated on the right). This is because the repulsion force between two modules depends on the position of the rotating masses in each vibration motor as well as on the friction of the rubber foam.

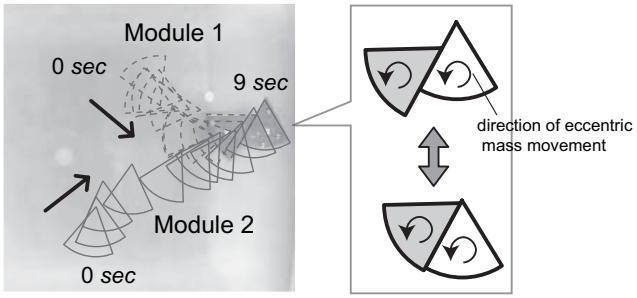

Figure 4: Trajectories of two modules during a 9-*sec* interval. Module 1 strikes module 2 while being attracted by the magnetic force between them. The illustration on the right shows that the relative positions of these two modules are unstable, depending strongly on the friction of the form rubber.

2.4 Aggregation behaviors

Snapshots taken during three experiments using 6 modules are shown in Figure 5 (see Extension 1). In each experiment, a different electric potential was applied between the ceiling plate and the immersed electrode causing the modules to aggregate in different ways.

In the experiment shown in Figure 5 (a), we applied a potential of $E = 7V$. The modules first moved along random paths in a manner vaguely reminiscent

of Brownian motion. After some time ($\approx 9\,sec$), due to the magnetic attraction, some of the modules were pulled together forming 2-clusters (denoted by X_2; X_k designates a cluster consisting of k modules). These clusters further combined to generate a 4-cluster (X_4), then a 5-cluster (X_5), and eventually a 6-cluster (X_6) (sequential aggregation). Once this final state was reached, the entire circular structure started to reform a propeller-like structure sliding the relative positions. This is due to the stability of the configuration when all remaining spaces were occupied by modules, which induced constant repulsive forces among them (note that each module repels its neighbor in the same direction, see Figure 4). Subsequently, this stable configuration causes synchronized contact of the pantographs to the ceiling, leading to a pulsed current flow. Consequently, the 6-cluster underwent a rotational movement.

In the snapshots reproduced in Figure 5 (b), the potential was set to $E = 8V$. As a result of the higher potential, the motors vibrated at a higher frequency, increasing the likelihood of breakup of clusters. Most of the time, all cluster types disintegrated shortly after formation, except for the 6-cluster (X_6) which, due to its symmetry, proved to be a stable structure. It is important to note that the formation of the 6-cluster at $98\,sec$ was accidental (here termed "one-shot aggregation"). This tendency of suppressing intermediate states is thought to be a potential solution to the yield problem (see Section 2.5). In Section 3, we focus on the characteristics of these two aggregation patterns and compare the results of numerical simulations.

The snapshots in Figure 5 (c) were obtained at a potential of $E = 9V$, which induced such rapid vibration that the formation of a 6-cluster became unlikely. In fact, even over prolonged experimental observation, no stable cluster was observed (random movements).

The experimental setup had a deficiency in keeping up the vibration motors speed at a high voltage ($8 - 9V$) for a long time because of self-generated heat. We confirmed these results by checking the stability of the circular configurations shown in (b) and (c) by performing 10 trials, each time initializing the experiment with 6 modules arranged in a circular configuration (the desired configuration). It was confirmed in all the cases that while at $8V$, the circular configuration remained stable, it broke up at $9V$. Considering that the tendency of segregations between two modules rises along with higher voltage supply, the described results seem probable. We further investigate this issue by modeling mathematical kinetic rate model in Section 3.

2.5 Yield problem

The problem of producing a desired configuration in large quantities (while avoiding incorrect assemblies) is known as the yield problem and has been studied in the context of biological and non-biological self-assembly systems (Hosokawa et al. 1994, 1996). As an example, let us assume that the self-assembly process is initialized with 7 modules. In fact, the likelihood that the system actually settles into the desired configuration (e.g. a circle) is rather low, and it is more likely that the kind of patterns shown in Figure 6 will occur. In this respect, suppressing the probability of producing stable intermediate states may help in reducing the occurrence of this problem, as is the case in Figure 5 b. We further investigate this issue in Section 3.

a) Sequential aggregation (E=7V).

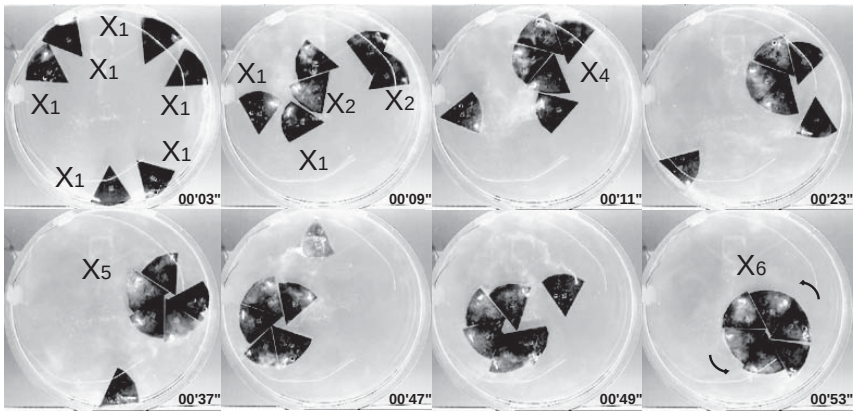

b) One-shot aggregation (E=8V).

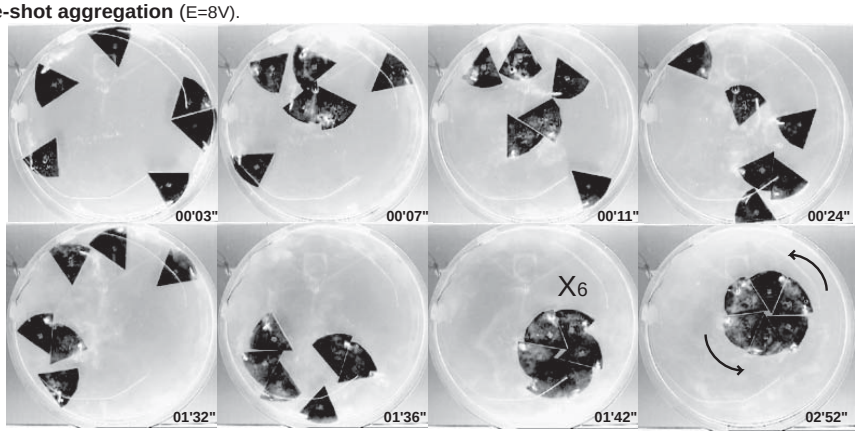

c) Random movements (E=9V).

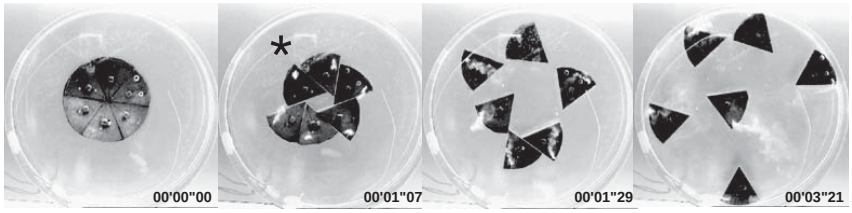

Figure 5: Experimental results. Self-assembly process as a function of applied electric potential E. (a) $E = 7V$, sequential aggregation. (b) $E = 8V$, "One-shot aggregation". (c) $E = 9V$, random movements. We checked the stability of the circular configurations shown in (b) and (c) by performing 10 trials beginning with circular configurations. It was observed that at $8V$, the circular configuration were stable, while it broke up at $9V$ (see Extension 1).

3 Chemical kinetic rate model

In order to quantitatively investigate the formation and stability of self-assembled circular-sector-shaped modules, a mathematical model was developed based on kinetic rate equations (Hosokawa et al. 1994; Gillespie 2007; Matthey et al. 2009;

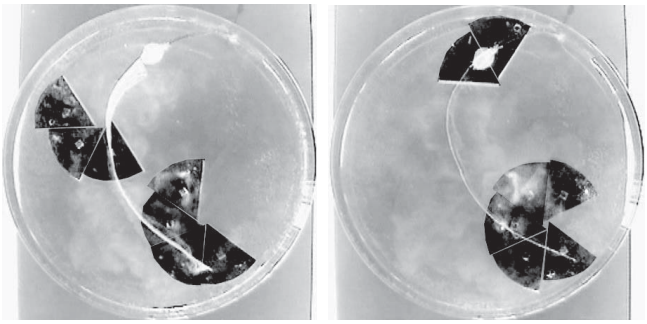

Figure 6: Yield problem and stable clusters. 7 circular sectors are placed in the arena. In most cases, however, the modules organize themselves in two clusters (cf. Section 4).

Mermoud et al. 2009). We employ the model to specifically study the global change of assembly patterns where a vast number of modules reside together, which is difficult to deal with in a real experiment. In this section, we call the conditions which correspond to the phenomena observed in Figure 5 a, b, (voltages of $7V$ and $8V$) "sequential aggregation" and "one-shot aggregation". The difference between them is that in the sequential aggregation process, a module should maintain its connection to a neighboring module once it has attached to it, while in the one-shot aggregation process, a single module may also disaggregate from a cluster at a constant speed (except for the stable configuration X_6, shown in Figure 5).

For the analysis, the intermediate products are represented by state variables. One can express the state transitions of the clusters as:

$$\begin{array}{lll} 2\mathrm{X}_1 \rightleftharpoons \mathrm{X}_2, & \mathrm{X}_1 + \mathrm{X}_2 \rightleftharpoons \mathrm{X}_3, & \mathrm{X}_1 + \mathrm{X}_3 \rightleftharpoons \mathrm{X}_4, \\ \mathrm{X}_1 + \mathrm{X}_4 \rightleftharpoons \mathrm{X}_5, & \mathrm{X}_1 + \mathrm{X}_5 \rightarrow \mathrm{X}_6, & 2\mathrm{X}_2 \rightarrow \mathrm{X}_4, \\ \mathrm{X}_2 + \mathrm{X}_3 \rightarrow \mathrm{X}_5, & \mathrm{X}_2 + \mathrm{X}_4 \rightarrow \mathrm{X}_6, & 2\mathrm{X}_3 \rightarrow \mathrm{X}_6 \end{array} \tag{13}$$

where X_k stands for the state of a cluster consisting of $k(\in 1, ..., 6)$ modules (e.g. two single modules X_1 can merge to form one cluster X_2). Reversible reactions are only possible in case of the one-shot aggregation. Note that we defined the transitions $2X_2 \rightarrow X_4$ and $X_2 + X_3 \rightarrow X_5$ to be irreversible, and X_6 to be the final state, since we seldom observed such disassembly in the experiments. The robustness of these clusters is mainly due to the geometrical stability of these configurations.

The transition of the state vector $\boldsymbol{x} = (x_1, \ldots, x_6)$, in which x_k denotes the average number of clusters consisting of k modules, obeys the following difference equation if x is large enough:

$$\boldsymbol{x}(t+1) = \boldsymbol{x}(t) + \boldsymbol{F}(\boldsymbol{x}(t)) \tag{14}$$

where t corresponds to the number of time steps, or more precisely, to the number of collisions between clusters. F_k is a transition function expressed as the sum of the products of (i) the collision probability P_{ij}^c $(i, j \in 1, ..., 6)$, the bonding probability P_{ij}^b, and the stoichiometric number ν_{ij} and (ii) the sum of the products of the disassembly probability $P_{i'}^d$ and stoichiometric number $\nu'_{i'}$,

namely:

$$F_k(x) = \sum_{i,j} \nu_{ij} P^c_{ij} P^b_{ij} + \sum_{i'} \nu'_{i'} P^d_{i'} x_{i'}, \tag{15}$$

where the stoichiometric numbers ν_{ij} (assembly) and $\nu'_{i'}$ (disassembly) are coefficients of the reaction seen in Eq. (13). The subscripts i and j in ν_{ij} denote the size of the two clusters assembling, and in $\nu'_{i'}$ the size of the disassembling cluster. The stoichiometric numbers correspond to the number of modules that make up the colliding clusters, and they have a positive sign if X_k is a product, and a negative sign if X_k is a reactant. Note that we are only interested in individual collision events. The model ignores the specific positions of the modules, assuming a well-mixed system.

The collision probability P^c_{ij} can be represented by Eq. (16), assuming that two clusters X_i and X_j are picked randomly in each time step (Hosokawa et al. 1994).

$$P^c_{ij} = \begin{cases} 2x_i x_j / (\sum_k x_k)^2 & (i \neq j) \\ x_i^2 / (\sum_k x_k)^2 & (i = j). \end{cases} \tag{16}$$

In Figure 7, two configurations consisting of circular-sector modules are shown. Here, S_k and M_k represent regions of the plane, and α, β, and γ represent angles in radians.

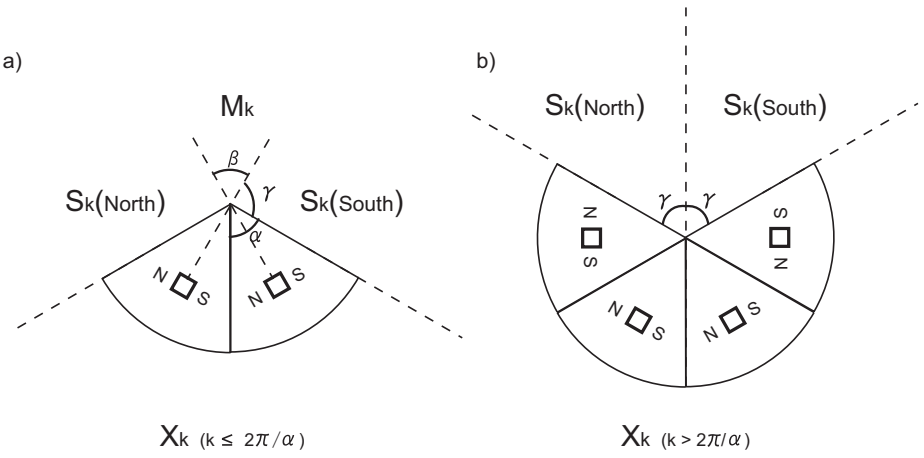

Figure 7: Two configurations consisting of circular-sector modules. α, β, and γ specify the corresponding angles, and $S_k(North), S_k(South)$, and M_k denote the specific regions referred to in Eq. (17). (a) The size of cluster is less than a half circle. (b) The size of cluster is more than a half circle.

Considering the geometric coordination, the conditional probability of bond-

ing when two modules X_i and X_j collide is given by

$$\begin{aligned} P_{ij}^b &= P((X_j \text{ in } S_i(South)) \cap (X_i \text{ in } (S_j(North) \cup M_j))) \cdot 2 \\ &\quad + P((X_j \text{ in } M_i) \cap (X_i \text{ in } (S_j(North) \cup S_j(South) \cup M_j))) \\ &= \begin{cases} \frac{\gamma_i}{2\pi} \cdot \frac{\beta_j+\gamma_j}{2\pi} \cdot 2 \; + \; \frac{\beta_i}{2\pi} \cdot \frac{\beta_j+2\gamma_j}{2\pi} & (i+j \leq \frac{2\pi}{\alpha}) \\ 0 & (i+j > \frac{2\pi}{\alpha}) \end{cases} \end{aligned}$$

where

$$\beta = \begin{cases} \alpha + (k-2)\alpha & (k \leq \frac{\pi}{\alpha}) \\ 0 & (k > \frac{\pi}{\alpha}) \end{cases}$$

$$\gamma = \begin{cases} \pi + (\frac{1}{2} - k)\alpha & (k \leq \frac{\pi}{\alpha}) \\ (2\pi - k\alpha)/2 & (k > \frac{\pi}{\alpha}) \end{cases} \tag{17}$$

and k represents the number of modules contained in the cluster. We assume that these modules will bond if (i) X_i is in the region $S_j(South)$ of X_j, and (ii) X_j is in the region $S_i(North)$ of X_i; i.e., if the magnetic north pole of module 2 (area N_2) faces the south pole of module 1 (area S_1) or vice versa.

P^d is set to zero for the case of sequential aggregation. In one-shot aggregation, we arrive at P^d using a model similar to the law of mass action used to describe chemical reactions. With the equilibrium constant K of the reaction $X_i + X_j \rightleftharpoons X_{i+j}$ being given by $K = k_+/k_-$, k_+ and k_- can be interpreted as the probability of bond formation and disassembly, respectively. With the bonding probability $\hat{P}^b$ set to the average of $\sum_j P_{1,j}^b$, K can be written as $K = \hat{P}^b/P^d = exp(\frac{-\Delta U'}{\rho v^2})$, where $\Delta U'$ is the energy of the bond formed between two modules. This means K grows exponentially with the bonding energy divided by the system's kinetic energy (Mermoud et al. 2009). We set this bond strength to be the normalized magnetic potential energy of a 2-cluster X_2 calculated with Eq. (5). ρv^2 is the mean energy of all the modules in our system, which have a Brownian-like motion. Since we cannot derive the total kinetic energy of the system, we set ρ to be a constant with units of s^2/m^5 and v^2 to have a value proportional to the systems' agitation. This leads to the probability of disassembly of a bond in the next time step to be $P^d = \hat{P}^b exp(\frac{\Delta U'}{\rho v^2})$. For further calculations we set $\rho = 1\, s^2/m^5$ and $v = 0.0232\, m/s$ (the mean velocity of the modules in our system). The disaggregation is set to occur in proportion to the number of each cluster. Taking the geometric configurations of each cluster into account, we set $P_2^d = P^d$, since there is only one bond that can be dissolved. We set $P_1^d = P_6^d = 0$, since the modules do not disassemble. For X_3 to X_5 clusters, we consider the leftmost or the rightmost module leaving the cluster (see Figure 7 (b)). Therefore we double the coefficient, namely setting $P_3^d = P_4^d = P_5^d = 2P^d$.

Finally we obtain F_k as:

$$
\begin{aligned}
F_1(\boldsymbol{x}) &= \{-2P^b_{11}x_1^2 - 2P^b_{12}x_1x_2 - 2P^b_{13}x_1x_3 - 2P^b_{14}x_1x_4 - 2P^b_{15}x_1x_5 \\
&\quad +2P^d_2x_2 + P^d_3x_3 + P^d_4x_4 + P^d_5x_5\}/(\sum_k x_k)^2 \\
F_2(\boldsymbol{x}) &= \{P^b_{11}x_1^2 - 2P^b_{12}x_1x_2 - 2P^b_{22}x_2^2 - 2P^b_{23}x_2x_3 - 2P^b_{24}x_2x_4 \\
&\quad -P^d_2x_2 + P^d_3x_3\}/(\sum_k x_k)^2 \\
F_3(\boldsymbol{x}) &= \{2P^b_{12}x_1x_2 - 2P^b_{13}x_1x_3 - 2P^b_{23}x_2x_3 - 2P^b_{33}x_3^2 \\
&\quad -P^d_3x_3 + P^d_4x_4\}/(\sum_k x_k)^2 \\
F_4(\boldsymbol{x}) &= \{2P^b_{13}x_1x_3 + P^b_{22}x_2^2 - 2P^b_{14}x_1x_4 - 2P^b_{24}x_2x_4 \\
&\quad -P^d_4x_4 + P^d_5x_5\}/(\sum_k x_k)^2 \\
F_5(\boldsymbol{x}) &= \{2P^b_{14}x_1x_4 + 2P^b_{23}x_2x_3 - 2P^b_{15}x_1x_5 \\
&\quad -P^d_5x_5\}/(\sum_k x_k)^2 \\
F_6(\boldsymbol{x}) &= \{2P^b_{15}x_1x_5 + 2P^b_{24}x_2x_4 + P^b_{33}x_3^2\}/(\sum_k x_k)^2. \qquad (18)
\end{aligned}
$$

3.1 Time evolution

Figure 8 shows the change over time of the yield of clusters, obtained by solving the system of difference equations described above with the initial condition $\boldsymbol{x}(0) = (100, 0, ..., 0)$. It shows the time evolution of the yield for the cases of sequential aggregation (a) and one-shot aggregation (b). In Figure 8 (a), only 38.9 % of modules aggregate into full 6-clusters, which exemplifies the yield problem. Also, since there is no means for the system to disaggregate, it becomes almost stagnant after a certain number of interactions, that is, only a few modules continue the assembly process. However, in Figure 8 (b), 99.0 % of modules aggregate to form 6-clusters. Note that the one shot self-assembly shown in (b) takes much longer to reach a stable state than the sequential aggregation in (a). In our calculations, increase of yields are observable when the probability of disaggregation P^d is in the range from 1.0×10^{-8} to 5.0×10^{-2}. In Figure 8 (c) and (d), we plot the trajectories of the time evolution of each cluster, where both the x and y axes represent yields (sequential aggregation model in (c) and one-shot aggregation model in (d)). In Figure 8 (c), we see that clusters consisting of 3, 4, and 5 modules are temporarily formed and subsequently decrease in number by converting to larger-sized clusters. The convergence in the values represented in (c) denotes yield problem (indicated with *). In Figure 8 (d), we see the convergence of all the intermediate states and the growth of the number of 6-clusters[2]. In Figure 8 (e), we compare the transition of the yield for the two conditions, where the improvement in yield is clearly shown.

[2]In the mathematical model, we did not consider the "bank-effect", in which many modules become stuck together on a wall and stop their dynamical motion.

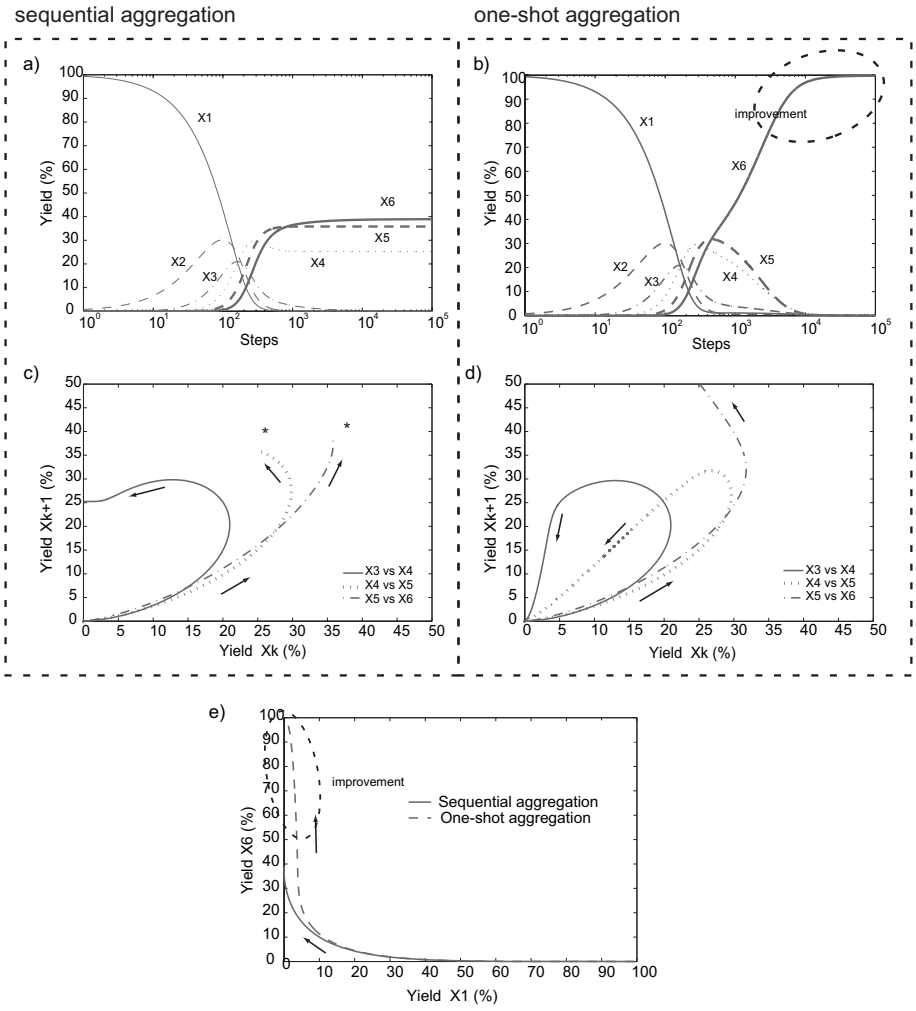

Figure 8: Change over time of the yield of clusters obtained by solving the model with the initial condition $\boldsymbol{x}(0) = (100, 0, ..., 0)$. (a, b) Time evolution of the yield for sequential aggregation (a) and one-shot aggregation (b). (c, d) Trajectories of time evolution of each cluster for sequential aggregation (c) and one-shot aggregation (d). (e) Comparison of the transition of yield under the two conditions. The convergence in the values represented in (c) denote yield problem (indicated with *).

The mechanism of one-shot aggregation is illustrated in Figure 9 (b), in contrast to sequential aggregation shown in Figure 9 (a). The core of one-shot aggregation is that the system happens to have a chance to configure a targeted formation (product) with a small probability, while processing reactions combined with aggregations and disaggregations. Also the condition that a product is more structurally stable than the other configurations must be met. We call it "one-shot aggregation" for the sake of easy understanding of the phenomenon. Note that we are fully aware of the fact that reverse reactions assisting in the growth of yield of a product can be frequently observed in chemistry. Our contribution is that we demonstrated the concept using a macroscopic physical

model.

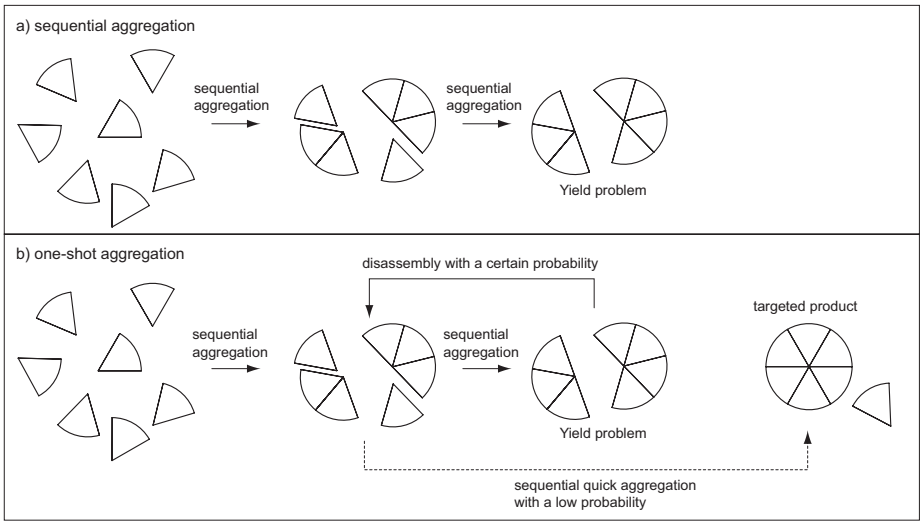

Figure 9: Mechanisms of aggregation. (a) Sequential aggregation leading to the yield problem. (b) One-shot aggregation leading to the increase of the targeted product.

The voltage (V) applied to the ceiling determines the level of perturbation introduced into the system. Thus it can be regarded as a kind of temperature (T) which is often employed as a control parameter in molecular self-assembly. The experimental results obtained show different voltages lead to different aggregation patterns. Moreover, by applying a large perturbation (e.g. $9\,V$), the system returns to its initial state, guaranteeing the reversibility of the reaction, which is a desirable property of our system. It allows the system to disaggregate undesired intermediate sub-assemblies.

3.2 Effect of morphology

In order to understand how the morphological properties of the modules influence the final state, we studied the stability of different configurations from the perspective of the magnetic potential energy. In Figure 10, we plot the normalized potential energy (U'_{total}) as a function of the position of the magnet in the module. In this case, we moved the magnet along the symmetry axis of the module and measured its distance to the vertex (a). The figure suggests that shifting the position of the magnet closer to the rounded edge causes the system to produce dimers (2-clusters) with the rounded edges touching (from Figure 10, the limit is $a \approx 34 \times 10^{-3}\ m$). In our experiments, $a = 25 \times 10^{-3}\ m$, which implies that the full circle cluster has minimal energy[3]. For reference, we also considered the case of a triangle configuration which was observed occasionally. The calculations confirmed that this is a rarely produced configuration.

Figure 11 shows how the change of the spanning angle of the corner affects the yield of the self-assembly process in sequential aggregation. The yields are

[3]This example seems to indicate that it is also possible to perceive this change not as a shift in the position of the magnet, but rather as a change in the entire mass distribution (morphology) from the "force source" (here: magnets).

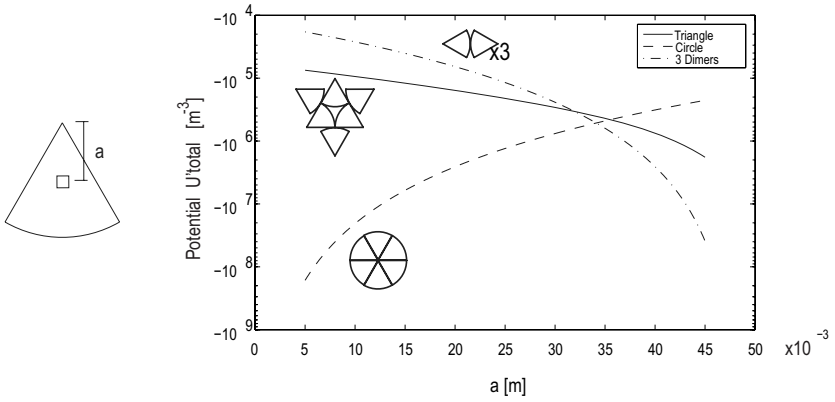

Figure 10: Potential energy of each configuration (full circle, 3 dimers, and triangular configuration) with respect to the distance of the magnet from the corner.

normalized by multiplying them by the number of modules required to construct a full circle (i.e., in the case of $\alpha = 60°$ the factor is 6; in the case of $\alpha = 180°$ the factor is 2), and plotted as a function of the angle α on a logarithmic scale. As can be seen in the figure, the narrower the angle becomes, the worse is the performance of the system. This result can be explained by considering that the number of clusters required to form the desired structure is inversely proportional to the angle. Interestingly, the relationship between yield and angle follows a power-law with a scaling exponent of 0.82. That is, the improvement of the yield saturates as the angle becomes wider. This result indicates that

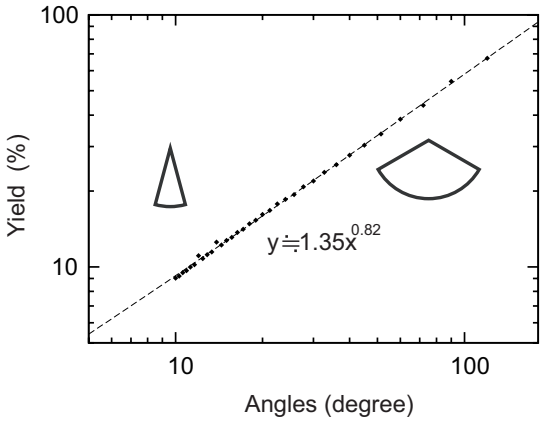

Figure 11: Yields as a function of the angle spanned by the circular-sector module in sequential aggregation. The relationship between yield and angle follows a power-law with a scaling exponent of 0.82.

there exists an optimal spanning angle for which both the aggregation rate and the number of identical modules can be maximized[4].

[4]In our circular-sector model, we considered the angle α to be an adequate parameter to measure the heterogeneity of the system. Although the 60° and 120° modules should be treated as different (heterogeneous) modules, once two 60° modules connect, a 120° module

4 Degree of parallelism

In a manufacturing process, the increase of yield is a critical factor in enhancing productivity and efficiency. As we will show in this section, the *degree of parallelism* can have a strong influence on the self-assembly processes. We introduce this quantitative measure to investigate the pattern of self-assembly focusing in particular on combinatorial matching patterns. The idea is to focus only on connections between components (neglecting the identity of each component), and to acquire information about the compounds. We now define the following variables:

x_i	number of connections within the i-th cluster
x_{comp}	number of connections in a complete cluster
X	number of all connections ($\equiv \sum_i x_i$)
X_{comp}	number of connections within the complete configuration of clusters ($\equiv \sum x_{comp}$)

To measure the geometrical connections of the modules, we define the local and global clustering degrees as:

Local clustering degree of i-th cluster	c_i	$\equiv \frac{x_i}{x_{comp}}$
Global clustering degree	C	$\equiv \frac{X}{X_{comp}}$.

Note that $C \neq c_i$ in general (see Figure 12). This measure allows us to characterize geometric topologies independent of the energy.

The *degree of parallelism* (DOP) H, as a function of the local clustering degrees (c_i), is used to quantify the aggregation paths (Miyashita et al. 2009), namely:

$$H = -\sum_{i=1}^{N} c_i \ln c_i. \tag{19}$$

Suppose that there exists a number N of clusters. From Shannon's lemma, it follows that the value H becomes maximum when the N clusters are all of the same size, namely:

$$\begin{aligned} H(X) &= -\sum_{i=1}^{N} c_i \ln c_i \\ &\leq -\sum_{i=1}^{N} \{\frac{1}{x_{comp}} \cdot \frac{X}{N}\} \ln\{\frac{1}{x_{comp}} \cdot \frac{X}{N}\} \\ &= -\frac{X}{x_{comp}} \ln\{\frac{1}{x_{comp}} \cdot \frac{X}{N}\}. \end{aligned} \tag{20}$$

The upper limit in Eq. (20), i.e. the maximal value for H, is obtained when $c_i = \{\frac{X}{x_{comp}} \cdot \frac{1}{N}\}$ for $\forall\, i$, that is, when there are equal numbers of clusters of the

forms, which is obviously equivalent to a 120° module. This example tells us that the concepts "homogeneous" and "heterogeneous" cannot be separated from the context in which they are used.

same size. This characteristic can be extended to general assembly processes, irrespective of the number of tiles or clusters.

The whole aggregation sequence can be quantified by the area covered by the DOP transition, namely:

$$H_{path} = \int_C H \, dC. \tag{21}$$

Figure 12 shows examples of clustering degrees with 6 modules in (a), and 12 modules in (b). The DOP of their intermediate states (left sides) are $H = 0.6452$ in (a), and $H = 1.2904$ in (b). Note that the DOP increases proportionately with the number of identical clusters. The concept can be extended and applied to assembly processes in general.

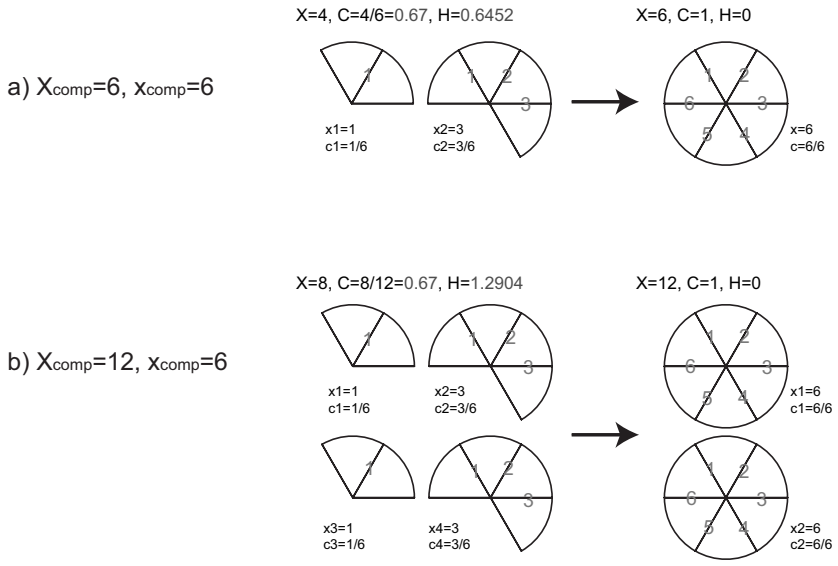

Figure 12: Examples of clustering degrees with 6 modules (a), and 12 modules (b). The DOP of their intermediate states (left sides) are $H = 0.6452$ in (a), and $H = 1.2904$ in (b). Note that DOP increases proportionately with the number of identical clusters.

4.1 The case of 6 modules

In Figure 13, the DOP as a function of the global clustering degree C is shown for the case of 6 modules. Considering the combination patterns, the probabilities of each transition are calculated and listed inside each path. The value P represents the probability of a state within the same C. For reference, the magnetic potential energies U are listed above each state.

The figure shows that as C increases, the DOP H increases, attaining a maximum for $C = 0.5$, and then decreasing to 0 for $C = 1$. Also, in each column (that is, within a group having the same number of connections), the more similar the clusters, the higher the DOP. In other words, high values are derived from states in which the connections are equally distributed. The highest DOP path (H_{path}), which goes through a state with $H = 0.8959$, has

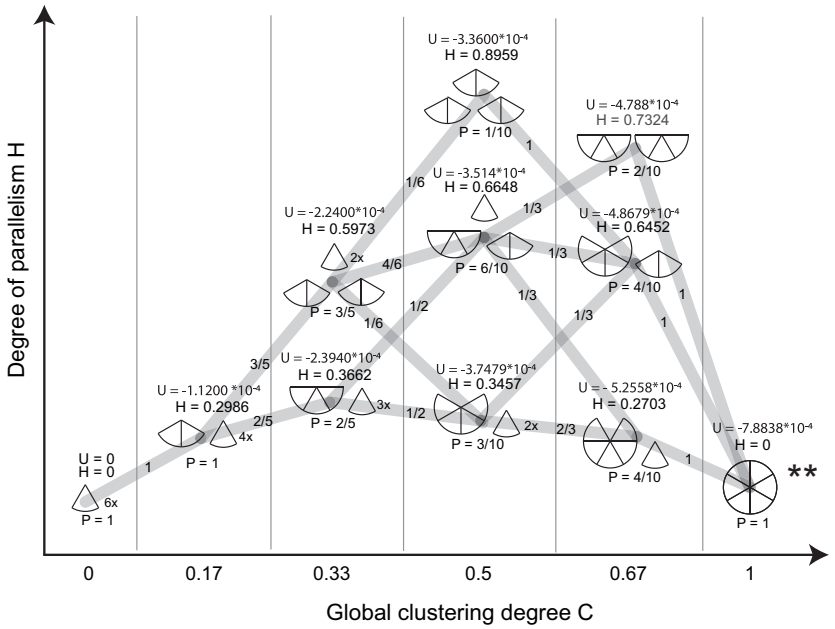

Figure 13: Change in DOP as a function of global clustering degree (6 modules). The more that assembly proceeds in parallel, the larger the value becomes. Note that the possible number of paths is 17 (without considering disassembly), and the reactions always produce a full circle (the final state is indicated with **).

a value of 0.461, while the lowest DOP path has a value of 0.236 (which goes through a state with the lowest H). Note that the possible number of paths is 17 (neglecting disassembly), and the reactions always produce a full circle (the final state is marked with a square).

4.2 The case of 7 modules

Conversely, the change in DOP for the case of 7 modules is shown in Figure 14. Surprisingly, the probability of configuring a full circle drops to 1/3 (the three possible final states are marked with squares). Other configurations with $4+3$ clusters and $5+2$ clusters are calculated to both occur with a probability of 1/3. This is a typical illustration of the yield problem associated with self-assembly processes. Here the total number of paths is 25, if we neglect disassembly.

5 Conclusion

This work showed an influence of reverse reactions on the improvement of yields of targeted products of stochastic self-assembly. By using a platform designed for the analysis of self-assembly systems, we observed a unique aggregation pattern at a specific stochasticity level - a number of modules instantly composed a product while avoiding converging to undesired geometric configurations. We hypothesized that this is mainly due to the disaggregation (reverse reaction) of undesired configurations that block the system, re-enabling modules to compose

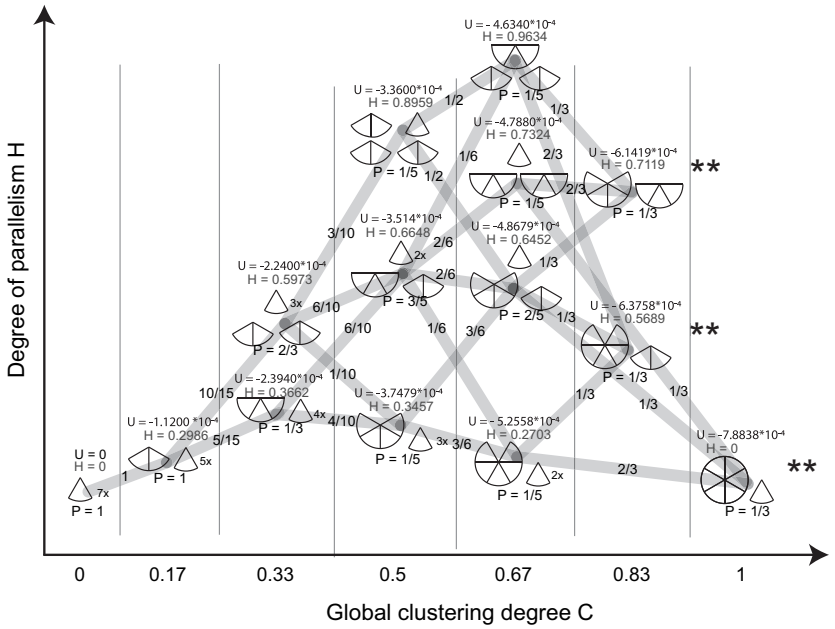

Figure 14: Change in DOP as a function of global clustering degree (7 modules). The probability of configuring a full circle drops to 1/3 (the three possible final states are indicated with **).

a product at a certain probability. We investigated the model using kinetic rate calculations and validated the hypothesis. In this regard, the discussion of the yield problem from a combinatorial perspective in Section 4 clearly depicts the causal reason. We believe this paper projects an insight on the macroscopic frame of chemical systems, and deepens the theoretical understanding to realize high efficient self-assembly robotic systems.

Appendix A: Index to Multimedia Extensions

The multimedia extension to this article is at: `http://www.ijrr.org`.

Extension	Media Type	Description
1	Video	Self-assembly processes shown in Figure 5

Acknowledgments

The authors sincerely thank Juan Pablo Carbajal, Max Lungarella, and Zoltàn Nagy for many useful inputs. We appreciate Rudolf Füchslin, and Peter Eggenberger Hotz for many helpful suggestions and for contributing their ideas to this paper. This research was supported by the Swiss National Science Foundation project (Scalable Self-Assembling Robots, #200020-118117).

References

Bishop, J., Burden, S., Klavins, E., Kreisberg, R., Malone, W., Napp, N., and Nguyen, T. (2005). Programmable parts: A demonstration of the grammatical approach to self-organization. In *IEEE/RSJ International Conference on Intelligent Robots and Systems (IROS)*, pp. 3684–3691.

Boncheva, M., Ferrigno, R., Bruzewicz, D. A., and Whitesides, G. M. (2003). Plasticity in self-assembly: Templating generates functionally different circuits from a single precursor. *Angewandte Chemie International Edition*, **42**: 3368–3371.

Bowden, N., Terfort, A., Carbeck, J., and Whitesides, G. M. (1997). Self-assembly of mesoscale objects into ordered two-dimensional arrays. *Science*, **276**: 233–235.

Castano, A., Behar, A., and Will, P. M. (2002). The conro modules for reconfigurable robots. *IEEE/ASME Transactions on Mechatronics*, **7**(4): 403–409.

Chirikjian, G. S. (1994). Kinematics of a metamorphic robotic system. In *IEEE International Conference on Robotics and Automation (ICRA)*, pp. 449–455.

Christensen, A. L., O'Grady, R., and Dorigo, M. (2007). Morphology control in a multirobot system. *IEEE Robotics & Automation Magazine*, pp. 18–25.

Fukuda, T. and Kawauch, Y. (1990). Cellular robotic system (CEBOT) as one of the realizations of self-organizing intelligent universal manipulator. In *IEEE International Conference on Robotics and Automation (ICRA)*, pp. 662–667.

Gillespie, D. T. (2007). Stochastic simulation of chemical kinetics. *Annual Review of Physical Chemistry*, **58**: 35–55.

Gracias, D. H., Tien, J., Breen, T. L., Hsu, C., and Whitesides, G. M. (2000). Forming electrical networks in three dimensions by self-assembly. *Science*, **289**: 1170–1172.

Griffith, S., Goldwater, D., and Jacobson, J. (2005). Robotics: Self-replication from random parts. *Nature*, **437**: 636.

Grzybowski, B. A., Stone, H. A., and Whitesides, G. M. (2000). Dynamic self-assembly of magnetized, millimetre-sized objects rotating at a liquid-air interface. *Nature*, **405**: 1033.

Grzybowski, B. A., Winkleman, A., Wiles, J. A., Brumer, Y., and Whitesides, G. M. (2003). Electrostatic self-assembly of macroscopic crystals using contact electrification. *Nature Materials*, **2**: 241–245.

Grzybowski, B. A., Radkowski, M., Campbell, C. J., Lee, J. N., and Whitesides, G. M. (2004). Self-assembling fluidic machines. *Applied physics letters*, **84**: 1798–1800.

Harada, K., Susilo, E., Menciassi, A., and Dario, P. (2009). Wireless reconfigurable modules for robotic endoluminal surgery. In *IEEE International Conference on Robotics and Automation (ICRA)*, pp. 2880–2885.

Hosokawa, K., Shimoyama, I., and Miura, H. (1994). Dynamics of self-assembling systems: Analogy with chemical kinetics. *Artificial Life*, **1**(4): 413–427.

Hosokawa, K., Shimoyama, I., and Miura, H. (1996). 2-d micro-self-assembly using the surface tension of water. *Sensors and Actuators A*, **57**: 117–125.

Jorgensen, M. W., Ostergaard, E. H., and Lund, H. H. (2004). Modular ATRON: Modules for a self-reconfigurable robot. In *IEEE/RSJ International Conference on Intelligent Robots and Systems (IROS)*, pp. 2068–2073.

Klavins, E. (2007). Programmable self-assembly. *IEEE Control System Magazine*, **27**: 43–56.

Kotay, K., Rus, D., Vona, M., and McGray, C. (1998). The self-reconfiguring robotic molecule. In *IEEE/RSJ International Conference on Intelligent Robots and Systems (IROS)*, pp. 424–431.

Leiman, P. G., Kanamaru, S., Mesyanzhinov, V. V., Arisaka, F., and Rossmann, M. G. (2003). Structure and morphogenesis of bacteriophage T4. *Cellular and Molecular Life Sciences*, **60**: 2356–2370.

Leong, T., Gu, Z., Koh, T., and Gracias, D. H. (2006). Spatially controlled chemistry using remotely guided nanoliter scale containers. *Journal of American Chemical Society*, **128**: 11336–11337.

Mao, C., LaBean, T. H., Reif, J. H., and Seeman, N. C. (2000). Logical computation using algorithmic self-assembly. *Nature*, **407**: 493–496.

Matthey, L., Berman, S., and Kumar, V. (2009). Stochastic strategies for a swarm robotic assembly system. In *IEEE International Conference on Robotics and Automation (ICRA)*, pp. 1751–1756.

Mermoud, G., Brugger, J., and Martinoli, A. (2009). Towards multi-level modeling of self-assembling intelligent micro-systems. In *International Conference on Autonomous Agents and Multiagent Systems (AAMAS)*, pp. 89–96.

Miyashita, S., Nagy, Z., Nelson, B. J., and Pfeifer, R. (2009). The influence of shape on parallel self-assembly. *Entropy*, **11**: 643–666.

Mondada, F., Gambardella, L. M., Floreano, D., Nolfi, S., Deneubourg, J.-L., and Dorigo, M. (2005). The cooperation of swarm-bots. *IEEE Robotics & Automation Magazine*, **12**: 21–28.

Murata, S., Kurokawa, H., and Kokaji, S. (1994). Self-assembling machine. In *IEEE International Conference on Robotics and Automation (ICRA)*, pp. 441–448.

Murata, S., Kurokawa, H., Yoshida, E., Tomita, K., and Kokaji, S. (1998). A 3-D self-reconfigurable structure. In *IEEE International Conference on Robotics and Automation (ICRA)*, pp. 432–439.

Murata, S., Tomita, K., Yoshida, E., Kurokawa, H., and Kokaji, S. (1999). Self-reconfigurable robot. In *International Conference on Intelligent Autonomous Systems (IAS)*, pp. 911–917.

Nagy, Z., Oung, R., Abbott, J. J., and Nelson, B. J. (2008). Experimental investigation of magnetic self-assembly for swallowable modular robots. In *IEEE/RSJ International Conference on Intelligent Robots and Systems (IROS)*, pp. 1915–1920.

Nakano, K., Uchihashi, S., Umemoto, N., and Nakagama, H. (1994). An approach to evolutional system. In *First IEEE Conference on Evolutionary Computation*, pp. 781 – 786.

Penrose, L. S. (1959). Self-reproducing. *Scientific American*, **200-6**: 105–114.

Rothemund, P. W. K. (2006). Folding DNA to create nanoscale shapes and patterns. *Nature*, **440**(7082): 297–302.

Rus, D. and Vona, M. (2001). Crystalline robots: Self-reconfiguration with compressible unit modules. *Autonomous Robots*, **10**(1): 107–124.

Saitou, K. (1999). Conformational switching in self-assembling mechanical systems. *IEEE Transactions on Robotics and Automation*, **15**: 510–520.

Seeman, N. C. (2003). DNA in a material world. *Nature*, **421**: 427–430.

Shih, W. M., Quispe, J. D., and Joyce, G. F. (2004). A 1.7-kilobase single-stranded DNA that folds into a nanoscale octahedron. *Nature*, **427**: 618–621.

Shimizu, M., Ishiguro, A., and Kawakatsu, T. (2005). A modular robot that exploits a spontaneous connectivity control mechanism. In *IEEE International Conference on Robotics and Automation (ICRA)*, pp. 2658–2663.

White, P., Kopanski, K., and Lipson, H. (2004). Stochastic self-reconfigurable cellular robotics. In *IEEE International Conference on Robotics and Automation (ICRA)*, pp. 2888–2893.

White, P., Zykov, V., Bongard, J., and Lipson, H. (2005). Three dimensional stochastic reconfiguration of modular robots. In *International Conference on Robotics Science and Systems (RSS)*, pp. 161–168.

Winfree, E., Liu, F., Wenzler, L. A., and Seeman, N. C. (1998). Design and self-assembly of two-dimensional DNA crystals. *Nature*, **394**(6693): 539 – 544.

Wolfe, D. B., Snead, A., Mao, C., Bowden, N. B., and Whitesides, G. M. (2003). Mesoscale self-assembly: Capillary interactions when positive and negitive menisci have similar amplitudes. *Langmuir*, **19**(6): 2206–2214.

Yim, M. (1994). New locomotion gaits. In *IEEE International Conference on Robotics and Automation (ICRA)*, pp. 2508–2514.

Yokoyama, T., Yokoyama, S., Kamikado, T., Okuno, Y., and Mashiko, S. (2001). Selective assembly on a surface of supramolecular aggregates with controlled size and shape. *Nature*, **413**: 619–621.

Zlotnick, A. (2005). Theoretical aspects of virus capsid assembly. *Molecular Recognition*, **18**(6): 479–490.

Zykov, V., Mutilinaios, E., Adams, B., and Lipson, H. (2005). Self-reproducing machines. *Nature*, **435**(7039): 163–164.